



Application of green synthesized nanocrystalline CuI in the removal of aqueous Mn(VII) and Cr(VI) ions

K. M. Archana¹ · D. Yogalakshmi¹ · Revathy Rajagopal¹

© Springer Nature Switzerland AG 2019

Abstract

Purging of heavy metals like chromium and manganese from water using various adsorbents is the need of the hour for our environment. Copper iodide nanoparticle (CuI NP) has garnered a lot of attention due to its singular physical and chemical properties. The present study reports the use of green synthesized CuI NP using *Hibiscus rosa-sinensis* L. flower extract which contains the anthocyanin, cyanidin-3-sophoroside (acts as both reducing and capping agents) in the removal of aqueous Cr(VI) and Mn(VII) ions. The synthesized CuI NP was characterized and was found to be nanocrystalline in nature, showing the presence of some surface crystal defects and having a high surface area making it a good adsorbent with adsorption capacities of 169.5 mg/g for Cr(VI) and 200 mg/g for Mn(VII) ions. The kinetics of metal removal was probed. The removal of metals was also probed using Freundlich and Langmuir adsorption models.

Keywords Green synthesis · Copper iodide · Adsorption studies · Heavy metal removal · *Hibiscus rosa-sinensis* L. · Adsorbent

1 Introduction

Nanosized particles synthesized by numerous methods have attracted extensive attention in recent years due to their potential use in abundant fields [1–5]. Water is one of the predominant needs for the survival and is also one of the abundant resources available on the earth. Even though two-thirds of the earth is filled with water, its scarcity is still a prevailing problem. One of the reasons for water crisis is also due to the increasing level of heavy metal pollution through rapid industrialization [6]. Several industries release huge amount of toxic effluents containing heavy metals, dyes, organic as well as inorganic impurities into the nearby aquatic streams without any treatment [7]. In recent times heavy metals are found to be one of the major environmental pollutants, which pose a risk to the environment [8]. Generally, high amount of Cr and Mn in

human body causes various diseases [9–12]. According to WHO, 0.01 mg/L and 0.05 mg/L are the permissible dose of Chromium and manganese, respectively, in potable water [13]. Although the literature reports [14] various adsorbents like activated carbon, hybrid inorganic nanocomposites, nanocrystalline polymers, etc., in the removal of Cr(VI) and Mn(VII) ions in water, most of them were found to end up in complications like solid–liquid separation, slow kinetics, low adsorption efficiency. Therefore, there is always a need for new, efficient and economically viable materials in this sector.

In the past few decades, copper iodide with its outstanding properties [15–20] has attracted many researchers with its applications in several fields [21–26]. Copper iodide has been reported to be prepared by various physical and chemical methods such as vacuum evaporation [27], deposition [28], low-temperature solvothermal

Electronic supplementary material The online version of this article (<https://doi.org/10.1007/s42452-019-0544-y>) contains supplementary material, which is available to authorized users.

✉ Revathy Rajagopal, revathyrajagopal@stellamariscollege.edu.in | ¹Department of Chemistry, Stella Maris College, Chennai 600 086, India.



SN Applied Sciences (2019) 1:522 | <https://doi.org/10.1007/s42452-019-0544-y>

Received: 28 December 2018 / Accepted: 29 April 2019 / Published online: 6 May 2019

synthesis [29], chemical extraction [30], etc. These methods can effectively fabricate copper iodide of uniform size and high crystalline grade, but the synthetic procedures are not free from disadvantages, as they require toxic raw materials, complicated synthetic steps, or high reaction temperature. It also includes methods that make use of chemical reducing agents which lead to environmental and biological risk. Hence, it is necessary to explore a clean, simplistic and environment friendly method to synthesize copper iodide nanoparticles under feasible conditions. Green synthesis is low cost, rapid, efficient and typically lead to the nanostructures with a variety of shapes. Recently, many researchers have attempted to synthesize copper iodide via green and ecologically friendly routes. These attempts comprise the utilization of plant or fruit extracts containing anthocyanins [31] as reducing agents, stabilizer and capping agent [32]. The present study aims at the synthesis of CuI NP using the *Hibiscus rosa-sinensis* L. flower extract and its use in the removal of aqueous Cr(VI) and Mn(VII) metal ions.

2 Experimental

2.1 Preparation of *Hibiscus rosa-sinensis* L. flower extract

Copper iodide nanoparticles were synthesized using flower extract of *Hibiscus rosa-sinensis* L. Flowers were collected from our college campus and washed several times with distilled water. The flower petals were separated and ground to a fine paste by adding distilled water. The paste was further diluted using water and centrifuged. The resultant centrifugate was used for synthesis.

2.2 Preparation of CuI NP (adsorbent)

AnalaR-Grade $\text{CuSO}_4 \cdot 5\text{H}_2\text{O}$ and KI were used without further purification. Copper iodide was prepared using the flower extract by a method as reported in the literature [19].

3 Material characterization

The synthesized copper iodide was characterized using X-ray powder diffraction (Bruker D8 advance P-XRD), scanning electron microscope (Carl Zeiss MA15/EVO18), energy-dispersive analysis of X-ray (Oxford INCA Energy 250 Microanalysis System), Fourier transform infrared spectroscopy (Bruker FTIR spectrometer, Alpha-T), UV-visible spectroscopy (Jasco UV-Vis Spectrophotometer, V-50), photoluminescence (Fluorolog-2500 fluorescence

spectrophotometer), and surface area analysis was done using Nova e2200 Quantachrome.

3.1 Cr(VI) and Mn(VII) adsorption batch experiments

For batch adsorption experiments, initially a stock solution of 1000 ppm of $\text{K}_2\text{Cr}_2\text{O}_7$ was prepared. Then, different dilutions (10 ppm to 100 ppm) of stock solution were prepared using distilled water and used as source of Cr(VI) ions. The same was repeated for Mn(VII) by diluting 1000 ppm stock of KMnO_4 . The λ_{max} was determined using UV-visible spectrophotometer by scanning 100 ppm solution over the wavelength range of 200–800 nm. The λ_{max} for Cr(VI) and Mn(VII) were found to be 375 nm and 527 nm, respectively. As the metal ions are adsorbed onto the surface of CuI, their concentration in bulk solution decreases. An equilibrium is reached between the metal ions on the surface of adsorbent and the bulk in a specific time. To determine the equilibrium concentration and time to reach equilibrium, the absorbance of each solution (10–100 ppm) was measured before addition of adsorbent and then equilibrated with 25 mg of CuI by stirring for 150 min. An aliquot of resulting solution was centrifuged and filtered, and absorbance was measured every 15 min up till 150 min. The remaining solution was kept at room temperature for equilibration. After 12 h, solution was filtered and absorbance of the filtrate was measured and found to be same as the absorbance of solution at the end of 2½ h, indicating the time of reaching equilibrium to be 2½ h. The equilibrium concentration was calculated from the absorbance measurement before and after adsorption as follows:

$$A_0 = \epsilon b C_0 \quad (1)$$

$$A_e = \epsilon b C_e \quad (2)$$

$$C_e = A_e / A_0 \quad (3)$$

where ϵ is specific absorptivity, b is path length, and C_0 and C_e are the initial and equilibrium concentrations of metal ion.

To quantify the upshot of pH and adsorption, the pH values of Cr(VI) solutions (10–100 ppm) were conformed to 2.0–8.0 by 0.1 M HCl or NaOH. Then, 25 mg of adsorbent was sprinkled to 50 mL of the solutions (10–100 ppm) under agitation for 150 min and placed for 12 h at ambient temperature. For the adsorption isothermal study, 25 mg of adsorbent was introduced to 50 mL solution from 10 to 100 ppm at a pH-value of 7.00 and 5.00 for Cr(VI) and Mn(VII), respectively. The solutions were persistently agitated for 150 min and placed for 12 h at room temperature. After every 15 min, the adsorbent was isolated from the mixture by centrifugation

and the ppm of metal ion adsorbed was determined using an UV-visible spectrophotometer. The amount of metal ion adsorbed/g of the adsorbent was appraised by using the following mass balance equation.

$$Q_t = (C_o - C_e)V/m \quad (4)$$

where q_t (mg g^{-1}) is the metal adsorbed/g of adsorbent, C_o (mg L^{-1}) the initial concentration of metal ion in the solution, C_e (mg L^{-1}) the equilibrium concentration of metal ions, V (L) the volume of the solution, and m the mass (g) of the adsorbent used. The filtered CuI after adsorption was later dried naturally and scanned between 4000 and 500 cm^{-1} to study the effect of metal adsorption on IR bands of copper iodide.

4 Results and discussion

CuI was synthesized using flower extract of *Hibiscus rosa-sinensis* L. It was observed that when 50 mL of 2 mmol solution each of $\text{CuSO}_4 \cdot 5\text{H}_2\text{O}$ and KI were mixed, there was no CuI formation, whereas when 2 mmol solution of $\text{CuSO}_4 \cdot 5\text{H}_2\text{O}$ containing *Hibiscus rosa-sinensis* L. flower extract was mixed with 2 mmol solution of KI, it resulted in CuI precipitate. The anthocyanins present in flower and fruit extracts are very good reducing agents. The anthocyanin in hibiscus flower is cyanidin-3-sophoroside; Fig. 1 represents the structure cyanidin-3-sophoroside. Therefore, the flower extract may be responsible for reduction of Cu^{2+} to Cu^+ , which forms CuI precipitate after reaction with KI. The yield of the synthesized product was found to be $\sim 75\%$.

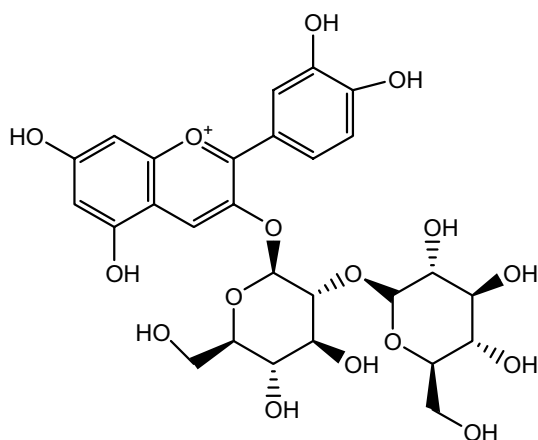


Fig. 1 Structure of cyanidin-3-sophoroside

4.1 X-ray powder diffraction

Copper iodide exists in three different phases α , β and γ ; out of the three phases, the gamma-phase is the most stable at room temperature. The X-ray powder diffraction (XRD) pattern of the synthesized compound was found to match well with that reported in the literature (JCPDS card no, 82-2111) for gamma-copper iodide [19]. The XRD pattern showed well defined peaks, implying that the compound is crystalline in nature. The slight broadening of the peaks may be attributed to the nanosize of the synthesized compound. The XRD data was found to fit in an fcc lattice of edge length $a = 6.0366 \text{ \AA}$. The following 2θ values 25.65° , 29.67° , 42.34° , 50.07° , 52.46° , 61.34° , 67.71° , 69.51° , 77.49° were indexed as represented in Fig. 2. In an fcc crystal system, the most intense peak is due to the (1,1,1) plane [33] and the indexed XRD pattern of CuI shows (111) as the most intense peak. Using Scherrer's formula, the mean crystallite size of copper iodide was calculated to be 89.1 nm. The nanocrystalline nature of the synthesized CuI particles may be due to the presence of capping layer of cyanidin-3-sophoroside, thereby preventing agglomeration of particles. The indexed x-ray powder diffraction data of CuI particles are provided in Table S1 of the electronic supplementary data.

4.2 Morphological studies

Morphology of the CuI nanoparticles were explored by SEM and EDAX analysis. SEM images revealed that the produced copper iodide nanoparticles appear to be stacked triangular flakes as shown in Fig. 3. Energy-dispersive X-ray spectroscopy analysis in Fig. 4 showed only the presence of elemental copper and iodine indicating high purity of the synthesized copper iodide nanoparticles. γ -CuI samples prepared by many experimental methods are reported to

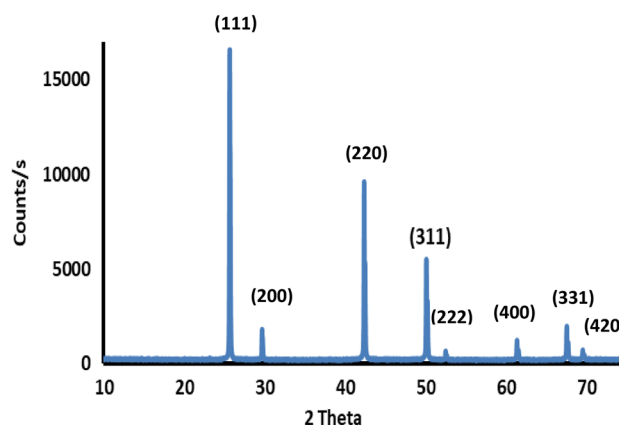


Fig. 2 XRD patterns of the copper iodide nanoparticles synthesized from *Hibiscus* flower extract

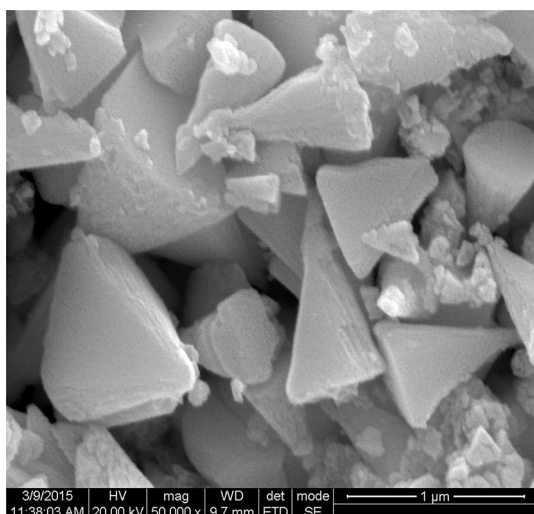


Fig. 3 SEM images of synthesized CuI

be of various dimensions, whereas the occurrence of an excess of Cu or I atoms in γ -CuI is highly unlikely [34]. The % atomic ratio as shown in Table 1 of Cu being slightly more than I may thus be attributed to the surface crystal defects in CuI making it a favorable adsorbent.

4.3 FTIR

The FTIR spectrum was scanned between 4000 and 500 cm^{-1} for the synthesized copper iodide nanoparticles and dried powder of flower *Hibiscus rosa-sinensis* L. Figure 5 represents the IR spectrum of CuI synthesized using flower extract and the extract of *Hibiscus rosa-sinensis* L.

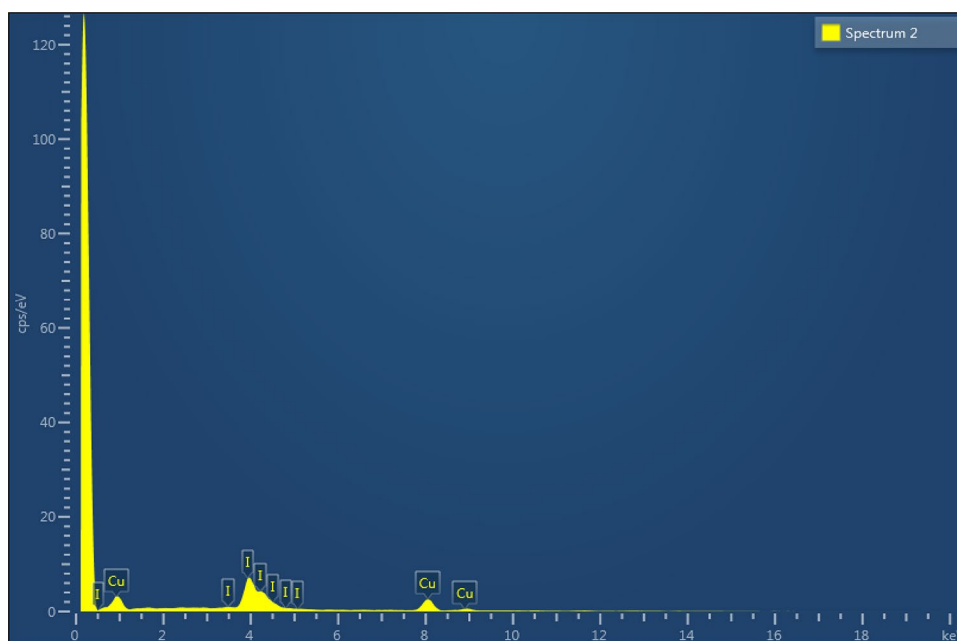
Table 1 Percentage composition of synthesized copper iodide from EDAX

Element	Line type	Weight (%)	Atomic (%)
Cu	K series	37.64	54.66
I	L series	62.136	45.34
Total		100	100

(containing cyanidin-3-sophoroside). The IR spectrum of pure CuI shows peaks at 622 and 457 cm^{-1} . The presence of characteristic IR bands of cyanidin-3-sophoroside in the IR spectrum of the synthesized copper iodide may be due to capping of CuI particles by cyanidin-3-sophoroside in the flower extract.

The flower extract contains the anthocyanin, cyanidin-3-sophoroside which acts a capping, stabilizing and reducing agent in the synthesis of copper iodide. The IR spectrum of the synthesized copper iodide using flower extract showed a shift in characteristic bands of cyanidin-3-sophoroside indicating the presence of bonding between them during capping. Table 2 shows the variation of force constant of various characteristic vibrational bands of functional groups of cyanidin-3-sophoroside and copper iodide synthesized using hibiscus flower extract containing cyanidin-3-sophoroside. As force constant is directly proportional to bond strength, the slight shift in force constants of various bonds may be due interaction between CuI and cyanidin-3-sophoroside. The stretching frequency at 3467 cm^{-1} may be due the phenolic O–H bond. The bands at 2921 and 2864 cm^{-1} correspond to C–H stretching and 1645 may be due to C=C stretching. The bands at 1263 cm^{-1} accords to in

Fig. 4 EDAX of synthesized CuI



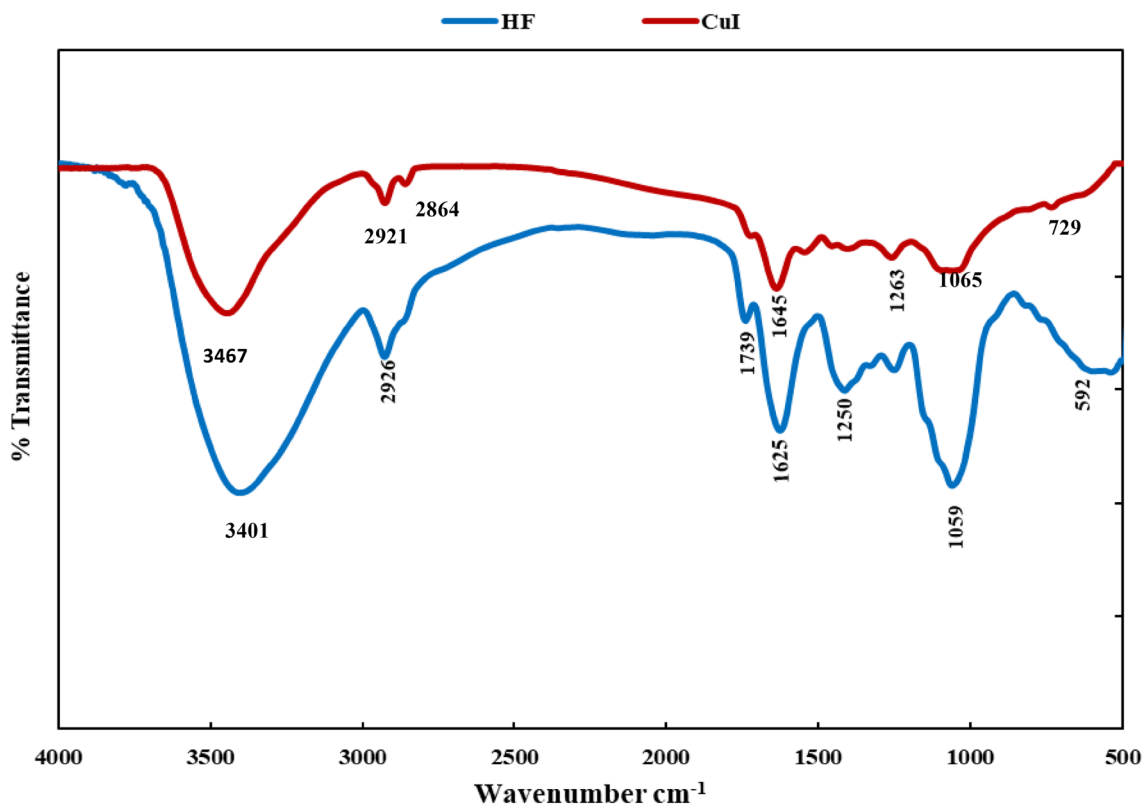


Fig. 5 FTIR spectrum of flower extract of *Hibiscus rosa-sinensis* L. (containing cyanidin-3-sophoroside) and synthesized copper iodide nanoparticle

Table 2 IR frequencies of synthesized copper iodide nanoparticles and cyanidin-3-sophoroside

Samples	Group	Wave number (cm ⁻¹)	Force constant (k) (N/m)
CuI	C–O	1065	457.94
	C–H	2864, 2921	444.28, 463.58
	O–H	3467	666.33
Cyanidin-3-sophoro-side	C–O	1059	452.70
	C–H	2926	465.11
	O–H	3401	640.73

plane C–H bending and a band at 729 cm⁻¹ may be due to =C–H out of plane bending seen only in CuI spectrum. The band 1065 cm⁻¹ corresponds to the phenolic C–O stretching.

4.4 UV–visible spectroscopy

The band gap of the synthesized copper iodide was calculated using the

Tauc equation, which is given in Eq. (5),

$$\alpha h\nu = C(h\nu - E_g)^{1/n} \tag{5}$$

In the above relation, α is the absorption coefficient, E_g the average band gap energy of the sample, and n is the type of transition. α is calculated using the following relation:

$$\alpha = \text{Absorbance} \times 2.303/t \tag{6}$$

where t is the thickness of the sample. For $n = 1/2$, E_g is the direct and allowed band gap. Figure 6 represents the Tauc plot of CuI. The value of the average band gap energy was calculated from the Tauc plot. The value of energy at $(\alpha h\nu)^2 \rightarrow 0$ was taken by extrapolating the graph and was found to be 2.90 eV which is less than that reported in the literature ~ 3.1 eV. This observation may be related to the defects shown by unequal distribution of Cu and I in EDAX, consequently resulting in lower band gap and increasing the number of active sites.

4.5 Photoluminescence spectra

Figure 7 shows the PL spectrum of copper iodide nanoparticle excited at 380 nm with an emission band at 420 nm corresponding to the band gap of 2.95 eV (blue shift). A blue shift from 2.86 to 2.95 eV may be related to the quantum confinement effect as expected for nanomaterials in

Fig. 6 Plot of $(\alpha h\nu)^2$ versus $h\nu$ Tauc plot

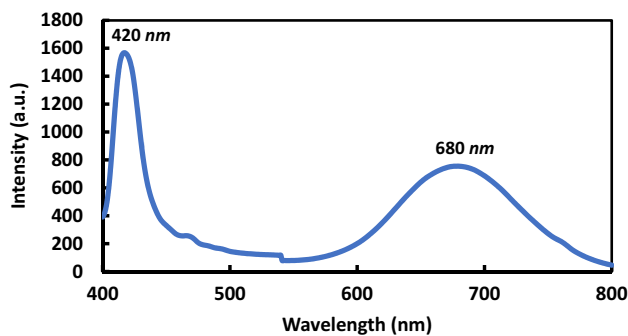
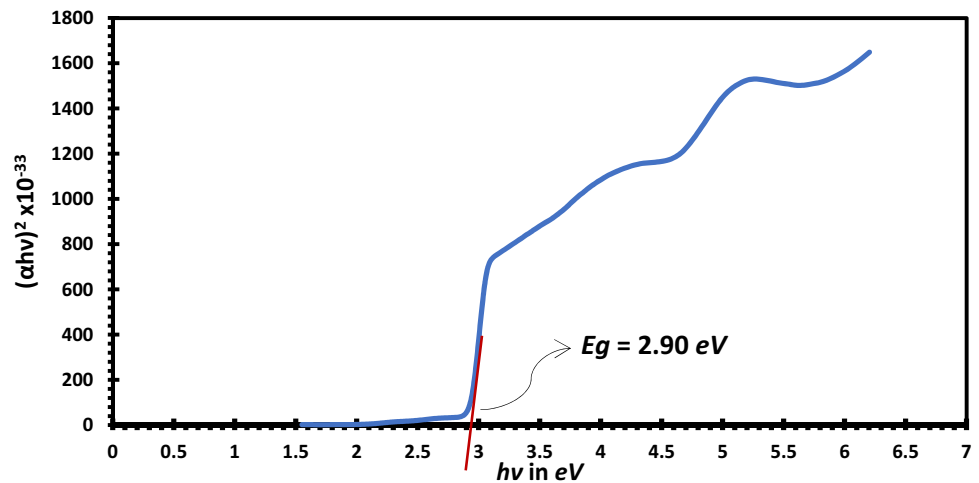


Fig. 7 The PL spectrum of synthesized copper iodide

PL spectra. The broad red luminescence centered at about 680 nm may be related to the iodine vacancy as reported in the literature [35, 36]. Hence, in line with the results from EDAX, PL studies also confirm the presence of defects in CuI.

4.6 Textural analysis

Adsorption process was understood by a graph of the quantity of adsorbate adsorbed onto the surface of the adsorbent and pressure of adsorbate at constant temperature. The CuI exhibited a type II isotherm, delineating the establishment of multilayer with no asymptote in the curve. The pore size distribution was scrutinized by Barrett–Joyner–Halenda (BJH) method. The surface area of CuI was observed to be $23.557 \text{ m}^2/\text{g}$, BJH pore diameter = 1.347 nm and pore volume = 0.038 cc/g . Thus, with a huge surface area the synthesized CuI can prove to be a useful adsorbent for removal of Cr(VI) and Mn(VII) ions. Sorption desorption curves in Figure S1 and BJH plot Figure S2 are provided in Supplementary data.

5 Metal ion removal by adsorption

In the batch adsorption experiments, the consequence of change in pH, contact time and incipient metal ion (in ppm) on the adsorption of metal ions (Cr(VI)/Mn(VII)) were investigated using green synthesized nanocrystalline CuI as adsorbent.

5.1 Cr(VI) removal

Initially, a stock solution of 1000 ppm of $\text{K}_2\text{Cr}_2\text{O}_7$ was prepared. Then, different dilutions of stock solution were prepared using distilled water and used as source of Cr(VI). The effect of initial chromium ion concentration, pH, adsorbent amount and contact time on adsorption (% metal removal) was probed.

5.1.1 Effect of initial concentration and pH

The consequence of primary concentration on % metal removal was calculated by using various dilutions (10–100 ppm) of stock potassium dichromate solution and 25 mg of CuI at room temperature. Each initial concentration of Cr(VI) reached equilibrium before $2\frac{1}{2}$ h. To determine the equilibrium concentration, the absorbance of each solution (10–100 ppm) was measured initially and then equilibrated with 25 mg of CuI by stirring for $2\frac{1}{2}$ h. At the end of $2\frac{1}{2}$ h, an aliquot of solution was centrifuged, filtered and absorbance measured. Then, the remaining solution was kept at ambient temperature for equilibration. At the end of 12 h, solution was filtered, and filtrate concentration was calculated from the absorbance measurement after adsorption. It was found that the absorbance at the end of $2\frac{1}{2}$ h and 12 h was same indicating the

attainment of equilibrium before 2½ h. Figures of solutions of metal ions before and after adsorption provided in Figure S3 and Figure S4 of the supplementary data.

Solution pH is a substantial controlling variable to the remove of metal ions since it judges the adsorbent charge density and oxidation states of the metal ion in solution. To probe the adsorption with the change of pH, the pH values of Cr(VI) solutions (10–100 ppm) were corrected to 2 to 8 by 0.1 M HCl or NaOH. Subsequently, 25 mg of adsorbent was mixed to 50 mL of the solutions, followed by 150 min of agitation and rest for 12 h at ambient temperature, then the resultant solutions were filtered. From the absorbance of the filtrate, amount of metal ions adsorbed was calculated using Eq. 4. Figure 8 refers to the effect of pH (2–8) for each initial Cr(VI) concentration.

Table 3 result indicates a high % of metal removal for low concentrations of Cr(VI) upto 30 ppm at pH 3, whereas beyond 40 ppm initial concentration of Cr(VI), the % metal removal decreases. The variation in % metal removal with pH can be expounded by considering the adsorbent surface charge and the ionization extent of the substances being adsorbed. Cr(VI) ions exist mostly as CrO₄²⁻ rather than HCrO₄²⁻ and/or, Cr₂O₇²⁻ anion forms in very dilute solutions.

In very dilute solutions up to 40 ppm, at lower pH, H⁺ are preferentially adsorbed and render positive charge to the surface sites of CuI nanocrystals. These are the sites where the negatively charged Cr(VI) species bind by showing high % of Cr removal. However, at pH 2, solubility of CuI samples would increase, thereby decreasing the number of active sites and consequently decreasing the % removal of metal ion. So, the Cr(VI) removal efficiency is reduced at pH 2.0.

On analyzing the % Cr(VI) removal at various pH and initial concentrations, it can be concluded that at pH 7 the % removal is good ranging from 30.76% for 10 ppm to 82.85% for 100 ppm initial Cr(VI) concentration. As OH⁻ is smaller in size and possesses higher mobility compared to ionized adsorbate ions at pH 8, the smaller OH⁻ may occupy the active sites preferentially, leading to a decrease in % metal removal. These results thus show that CuI displayed good adsorption properties of removing Cr(VI) at pH 7.0. The IR spectrum of CuI before and after adsorption of metal ions was scanned between 4000 and 500 cm⁻¹.

The IR spectra of CuI before and after adsorption show a slight shift in bands as represented in Fig. 9 indicating the adsorption of metal ions on the surface due to which three main bands show shift. The force constants calculation also

Fig. 8 Plot of % removal of Cr(VI) ion of initial concentrations (10–100 ppm) at pH 2 to 8

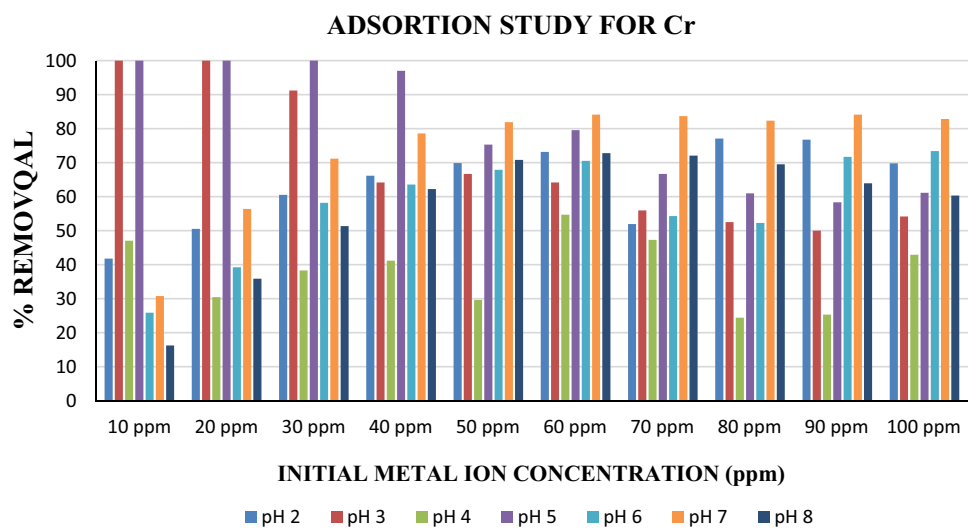
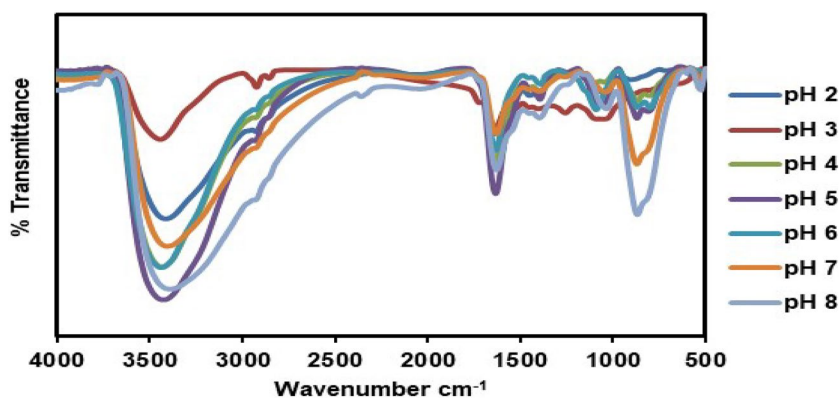


Table 3 Removal % of Cr(VI) ion of initial concentrations (10–100 ppm) at pH 2 to 8

ppm pH	10	20	30	40	50	60	70	80	90	100
2	41.77	50.50	60.52	66.16	69.86	73.17	51.95	77.08	76.77	69.78
3	100	100	91.22	64.17	66.66	64.15	55.93	52.51	50.00	54.18
4	47.05	30.43	38.29	41.17	29.62	54.68	47.29	24.39	25.27	42.92
5	100	100	100	97.01	75.32	79.56	66.66	60.97	58.33	61.14
6	25.86	39.24	58.16	63.55	67.88	70.51	54.28	52.28	71.68	73.41
7	30.76	56.41	71.18	78.57	81.90	84.12	83.67	82.35	84.12	82.85
8	16.21	35.84	51.31	62.24	70.80	72.78	72.06	69.51	63.94	60.33

Fig. 9 IR spectrum CuI before and after adsorption of Cr(VI) ion



shows a decrease in its value which may be due to adsorption of metal ion on the surface. Calculated force constants from IR data before and after adsorption are provided in Table S2 the electronic supplementary data

5.1.2 Effect of adsorbent dosage

Since the adsorption of Cr shows good results at pH 5 and 7, the effect of adsorbent dosage study was done at pH 5 and 7. The % purging of Cr by CuI at differing adsorbent doses (5, 15, 25, 35 and 45 mg) for the chromium concentration 100 ppm was investigated. The results showed that the % removal of Cr(VI) increases rapidly with CuI dosage from 5 to 45 mg at both the pH which probably could be due to the greater accessibility of active sites on the surface of the adsorbent.

The removal efficiency increased from 17.88 to 77.48% at pH 5 and from 27.18 to 88.47% at pH 7 as represented in Table 4. As Cr(VI) removal efficiency was more at pH 7, consequence of contact time on % Cr(VI) removal was studied using 100 ppm initial concentration at pH 7.

5.1.3 Effect of contact time

Contact time is a crucial factor affecting metal ion removal in solution. The effect of contact time on the adsorption of Cr(VI) ions in solution was carried out by taking 50 ml of

Table 4 Effect of adsorbent dosage on Cr(VI) ion removal at pH 5 and 7

Adsorbent dosage (mg)	% Removal Cr pH 5	% Removal Cr pH 7
5	17.88	27.18
15	31.78	42.39
35	57.61	82.94
35	70.86	85.71
45	77.48	88.47

100 ppm Cr(VI) solution at pH 7 and 25 mg of CuI, and the resultant solution was stirred continuously. Absorbance of aliquots of this mixture was measured every 15 min for 150 min.

It can be seen from Table 5 and Fig. 10 that as time increased, the % removal of metal ions also increased fast initially and then gradually to reach a maximum at equilibrium beyond 120 min. The quantity of metal ion adsorbed in mg/g 'qt' of the adsorbent at a time t was determined by utilizing the balance Eq. (4). The qt obtained at equilibrium corresponds to the absorption capacity of CuI for Cr removal and was found to be 169.46 mg/g (emphasised in bold in Table 5).

5.2 Mn(VII) removal

Initially, a stock solution of 1000 ppm of $KMnO_4$ was prepared. Then, different dilutions of stock solution 10–100 ppm were prepared using distilled water and used as source of Mn(VII). The effect of initial concentration of metal ion, pH, amount of adsorbent and contact time on adsorption (% removal of metal) was probed.

Table 5 Effect of contact time for % Cr(VI) removal at pH 7

Contact time (min)	% Cr removal	q_t (mg/g)
0	0	0
15	15.26	30.52
30	25.19	50.38
45	26.20	52.40
60	27.22	54.44
75	53.18	106.36
90	59.28	118.56
105	83.71	167.42
120	84.73	169.46
135	84.73	169.46
150	84.73	169.46

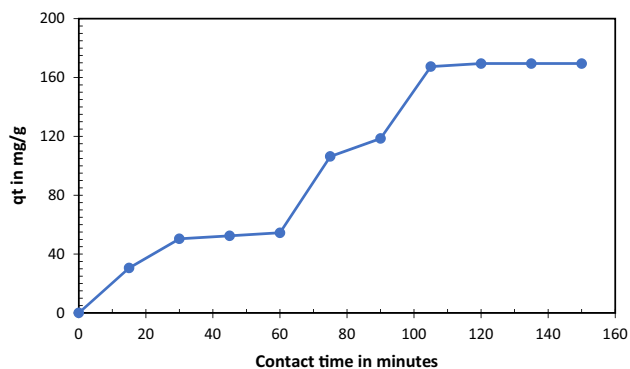


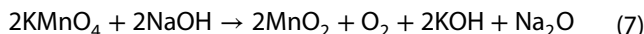
Fig. 10 Plot of contact time and adsorption capacity 'qt' of Cr at pH 7

5.2.1 Effect of initial concentration and pH

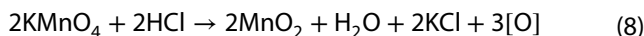
The effect of initial concentrations and pH of Mn(VII) on % metal removal using CuI as adsorbent was probed by procedures like Cr(VI) removal. The results of effect of pH

and initial concentration of Mn(VII) on % Mn removal are represented in Table 6 and Fig. 11.

It is observed that with the increase in initial concentration and pH, % metal removal increased in most of the cases; this can be attributed to the adsorption of ionized MnO_4^- and reduced MnO_2 in the solution of pH less than 7. At pH more than 7, the adsorption decreased slightly owing to reduction according to Eq. (7)



It was observed that the solution turned brownish at the end of 12 h with a rise in initial concentration of Mn(VII) and pH; this may be due to reduction of MnO_4^- ions to MnO_2 according to Eq. (8)

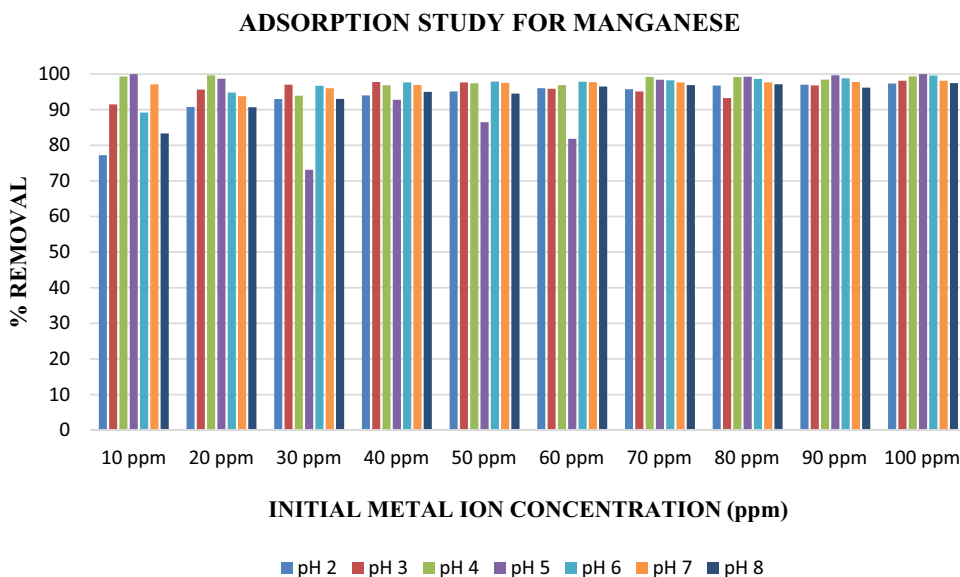


The IR spectrum of CuI before and after adsorption of Mn(VII) ion was scanned between 4000 and 500 cm^{-1} . The IR spectra of CuI before and after adsorption showed a slight shift in bands as represented in Fig. 12, indicating the adsorption of metal ions on the surface. Calculated force constants from IR data before and after adsorption

Table 6 Removal % of Mn(VII) ion of initial concentrations (10–100 ppm) at pH 2 to 8

ppm pH	10	20	30	40	50	60	70	80	90	100
pH 2	77.21	90.78	92.97	94.03	95.12	96.03	95.75	96.78	97.02	97.33
pH 3	91.46	95.63	97.00	97.76	97.67	95.86	95.10	93.27	96.84	98.11
pH 4	99.33	99.64	93.92	96.85	97.41	96.91	99.21	99.15	98.45	99.37
pH 5	100	98.69	73.11	92.80	86.51	81.84	98.42	99.23	99.69	100
pH 6	89.18	94.82	96.69	97.67	97.88	97.84	98.25	98.63	98.81	99.58
pH 7	97.10	93.77	96.02	96.94	97.53	97.75	97.67	97.67	97.76	98.13
pH 8	83.33	90.69	93.01	95.00	94.51	96.5	96.90	97.12	96.18	97.47

Fig. 11 Plot of % removal of Mn(VII) ion of initial concentrations (10–100 ppm) at pH 2 to 8



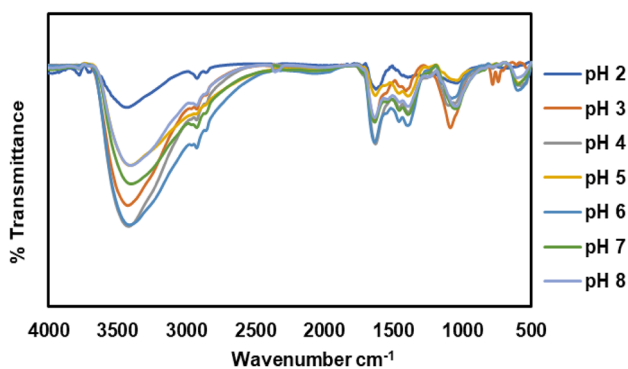


Fig. 12 IR spectrum of CuI before and after adsorption of Mn(VII) ion

of Mn(VII) are provided in Table S3 of the electronic supplementary data.

5.2.2 Effect of adsorbent dosage

The consequence of amount of adsorbent on adsorption was probed using 100 ppm Mn(VII) solution at pH 5 as the percent removal of metal ion was good at pH 5.

The % removal of Mn(VII) using CuI at different adsorbent doses (5, 15, 25, 35 and 45 mg) for the 100 ppm Mn(VII) solution was investigated, and the results are represented in Table 7. It can be observed that % Mn(VII) removal reaches maximum for 25 mg of adsorbent and then it decreases since at high adsorbent dosage aggregation of adsorbent occurs, resulting in the decrease in active sites as electrostatic interferences dwindled attractions between the adsorbing solute and the superficies of the adsorbent. Thus, 25 mg of CuI was used for % Mn removal at pH 5 for probing effect of contact time on metal removal.

5.2.3 Effect of contact time

The effect of contact time on the adsorption of Mn(VII) ions in solution was done by taking 50 ml of 100 ppm Mn(VII) solution at pH 5 and 25 mg of CuI. The resultant solution

Table 7 Effect of adsorbent dosage for % removal Mn(VII) ion at pH 5

Adsorbent dosage (mg)	% Removal of Mn at pH 5
5	51.89
15	99.92
25	100
35	99.03
45	97.51

Table 8 Effect of contact time for % removal Mn(VII) ion at pH 5

Contact time (min)	% Removal of Mn(VII)	q_t
0	0	0
15	84.00	168
30	89.31	178.62
45	91.91	183.82
60	92.32	184.62
75	95.02	190.04
90	95.75	191.5
105	96.00	192
120	100	200
135	100	200
150	100	200

was stirred continuously. The % metal removal was studied every 15 min for 150 min. Table 8 shows the effect of contact time on % Mn(VII) removal at a time interval range 0 to 150 min. The results show that the rate of uptake is fast and reaches about ~85% at the first 15 min. The equilibrium is attained at the 150th min. It showed that during adsorption of Mn(VII) ions, the primary step drives to surface adsorption of Mn on the surface of CuI adsorbent due to availability of more active sites, the subsequent step leads to intraparticle transit from bulk fluid to the external surface of the permeable adsorbent. Thus, in the first phase, all the adsorption sites on the adsorbent surface are available which resulted in the faster removal of metal ion from solutions, and the second phase might be due to the obstruction of the pores by the manganese ions. Generally, % metal removal increased with an increase in contact time till equilibrium is reached and after which it remained constant. A plot of q_t the amount adsorbed in mg/g of adsorbent verses time gives adsorption capacity at equilibrium is shown in Fig. 13. The adsorption capacity

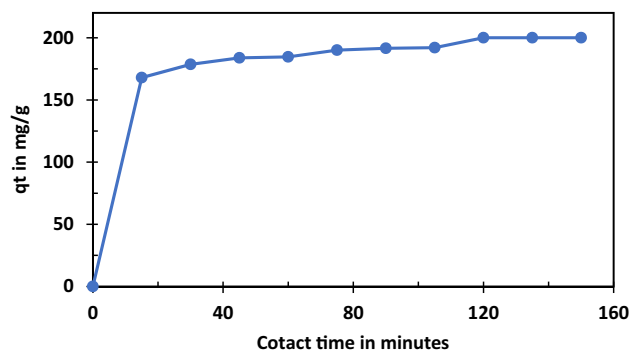


Fig. 13 Plot of contact time and adsorption capacity ' q_t ' of Mn(VII) at pH 5

is detected to be 200 mg/g of adsorbent (emphasised in bold in Table 8).

5.3 Adsorption kinetics

The adsorption kinetic models are prominent in the operation of purging of deleterious heavy metals from the aqueous medium. In the present study pseudo-first- and pseudo-second-order models were examined. The sorption kinetics following the pseudo-first- and pseudo-second-order reaction model was calculated using Eqs. (9) and (10)

$$\ln(q_e - q_t) = \ln q_e - k_1 t \quad \text{pseudo-first order} \quad (9)$$

$$t/q_t = 1/k_2 \cdot q_e^2 + (1/q_e) t \quad \text{pseudo-second order} \quad (10)$$

where 'q_e' is the amount of solute adsorbed at equilibrium/g of adsorbent (mg g⁻¹), 'q_e - q_t' is the amount of solute adsorbed at any moment 't', and 'k₁' is the rate constant. From the plots of ln (q_e - q_t) versus t and 1/q_t versus 1/t, the pseudo-first-order and pseudo-second-order rate constants, respectively, were calculated.

From R², it can be inferred that adsorption of Mn(VII) on adsorbent CuI follows pseudo-second-order kinetics and that of Cr(VI) follows pseudo-first-order kinetics with rate constants as reported in Table 9 (conclusions are re-emphasised in bold).

5.4 Adsorption models

Two probative equations, the Langmuir (Eq. 11) and Freundlich isotherm (Eq. 12) models, were used to analyze the adsorption data.

$$1/q_e = 1/q_m + (1/q_m \cdot b) (1/C_e) \quad (11)$$

$$q_e = kC_e^{1/n} \quad (12)$$

where C_e is the equilibrium ppm of Cr(VI) ion (mg L⁻¹), q_e the equilibrium adsorption capacity (mg g⁻¹), q_m (mg g⁻¹)

Table 9 Pseudo-first- and pseudo-second-order constants

Metal ions	k ₁ (min ⁻¹)	R ²	k ₂ (L min ⁻¹ g ⁻¹)	R ²
Cr(VI)	0.03132	0.9151	2.14 × 10 ⁻⁵	0.312
Mn(VII)	0.025	0.7674	2.769 × 10⁻³	0.9984

and b (mg L⁻¹) are constants allied to the maximum adsorption scope and energy of adsorption, respectively, and k and 1/n are the constants of Freundlich adsorption isotherm. Table 10 shows the constants of Langmuir and Freundlich adsorption isotherm models as observed for removal of Cr(VI) and Mn(VII) ions using CuI as adsorbent. It is indicated that based on R² values (emphasised in bold in Table 10), Cr(VI) removal fitted better in Freundlich adsorption model, whereas Mn(VII) removal was found to fit well in Langmuir adsorption model. The value of 1/n less than one indicates chemisorption process, while that of unity indicates partition between the liquid phase and solid phase are independent of concentration and the value of 1/n above unity exhibits cooperative adsorption (emphasised in bold in Table 10) [37]. Tables and figures related to calculation of Freundlich adsorption constants and Langmuir constants are provided in Table S4 and Figures S5 and S6(Cr) and S7 and S8 (Mn) of the electronic supplementary data.

Table 11 Adsorption capacities of different adsorbents for chromium and manganese

Adsorbents	Adsorption capacity (mg/g)		References
	Cr	Mn	
Activated rice husk carbon	0.8	-	[38]
Activated alumina	1.6	-	[38]
γ-Fe ₂ O ₃	17.0	-	[39]
Nano-Al ₂ O ₃	8.56	-	[40]
Dolomite	10.01	-	[41]
Nano-MnFe ₂ O ₄	31.55	-	[42]
Sulphonated lignite	27.87	-	[43]
AC/f-MWCNTs	113.29	-	[44]
AC/f-CNSs	105.48	-	[44]
Tannic acid immobilized activated carbon	-	1.13	[45]
Natural zeolitic tuff	-	10.0	[46]
Magnetic graphene oxide	-	16.5	[47]
Thermally decomposed leaf	-	66.57	[48]
Pithacelobium dulce carbon	-	0.415	[49]
Crab shell particles	-	69.9	[50]
Pecan nutshell biosorbent	-	103.8	[51]
Nano-Cul	169.5	200	Present study

Table 10 Freundlich and Langmuir adsorption isotherm analyses

Metal ions	Freundlich constants			Langmuir constants		
	1/n	K (mg g ⁻¹ /(L mg ⁻¹))	R ²	q _m (mg g ⁻¹)	b (L mg ⁻¹)	R ²
Cr(VI)	1.523	2.4664	0.7786	22.779	0.4516	0.4852
Mn(VII)	0.42	3.5 × 10 ⁻⁴	0.412	2500	26.5	0.988

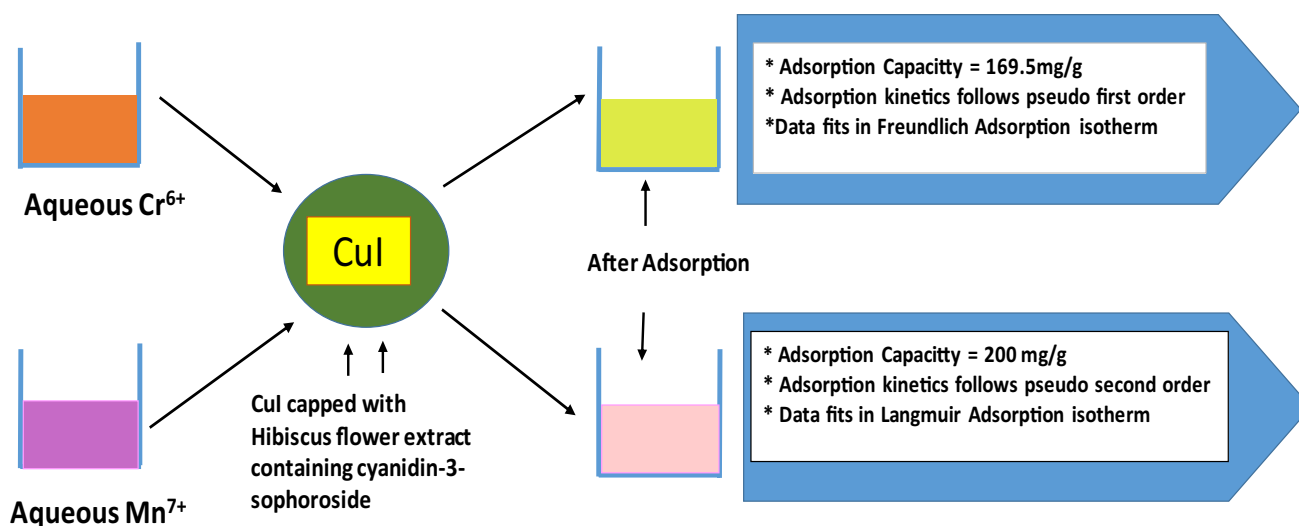


Fig. 14 Application green synthesized CuI in removal of aqueous Cr⁶⁺ and Mn⁷⁺ ions

Cr(VI) and Mn(VII) removal capacities of CuI nanocrystals were found to be 169.5 mg g⁻¹ and 200 mg g⁻¹, respectively. These values were much greater than adsorption capacities of Cr(VI) and Mn(VII) removal using other adsorbents. Table 11 shows the reported adsorbents for the removal of Cr(VI) and Mn(VII) ions.

6 Conclusion

The green synthesized copper iodide nanoparticles using *Hibiscus rosa-sinensis* L. flower extract was found to be γ -CuI of nanocrystalline nature of approximate size 89.1 nm and fitted well in an FCC lattice of edge length 6.0366 Å. The anthocyanin, cyanidin-3-sophoroside present in *Hibiscus rosa-sinensis* L. extract acts as reducing and capping agent. The infrared spectrum of the CuI nanocrystal shows characteristic bands indicating the presence of cyanidin-3-sophoroside. The SEM EDAX data of synthesized CuI showed that copper iodide was pure and the presence of slight unequal distribution of Cu⁺ and I⁻ may be due to some surface defects making it a good adsorbent. The UV-visible spectrum and photoluminescence also confirmed the presence of defects in the synthesized CuI. The removal of aqueous Cr(VI) and Mn(VII) using CuI as adsorbent gave adsorption capacities of 169.5 and 200 mg/g, respectively, which is much higher than that of the other adsorbents published in the literature. The nanocrystalline nature, presence of defects and high surface area make the green synthesized CuI a good adsorbent. The adsorption for Cr(VI) was observed to follow pseudo-first-order kinetics

and Mn(VII) was found to follow pseudo-second-order kinetics. In adsorption models, Mn(VII) removal fitted in Langmuir adsorption isotherm model and Cr(VI) removal fitted well in Freundlich adsorption isotherm model. Figure 14 gives an outline of the present work.

Acknowledgements All the authors appreciate the solid support of Dr. Harinipriya Seshadri, Scientist, SRM Research Institute, Katankalathur, Kanchipuram District, Tamilnadu. We gratefully acknowledge CRIST lab, Stella Maris college, Chennai; P-XRD lab, Department of Chemistry, IIT-Madras; Crystal Growth Centre, Anna University, Chennai, for their help in SEM characterization.

Compliance with ethical standards

Conflict of interest The authors declare that they have no conflict of interest.

References

- Li P, Fan H, Cai Y (2013) In₂O₃/SnO₂ heterojunction microstructures: facile room temperature solid-state synthesis and enhanced Cl₂ sensing performance. *Sensors Actuators B Chem* 185:110–116. <https://doi.org/10.1016/j.snb.2013.05.010>
- Li J, Fan H, Chen X (2009) Structural and photoluminescence of Mn-doped ZnO single-crystalline nanorods grown via solvothermal method. *Colloids Surf A* 349(1–3):202–206. <https://doi.org/10.1016/j.colsurfa.2009.08.019>
- Lu D, Zhang X, Wang S, Peng W, Fan H, Hao H et al (2019) Enhanced photocatalytic removal of Cr(VI) over 0D/2D anatase/graphene and its synergism with organic pollutants under visible light irradiation. *Appl Surf Sci* 470:368–375. <https://doi.org/10.1016/j.apsusc.2018.11.145>
- Wang C, Fan H, Ren X, When Y, Wang W (2018) Highly dispersed PtO nanodots as efficient co-catalyst for photocatalytic

- hydrogen evolution. *Appl Surf Sci* 462:423–431. <https://doi.org/10.1016/j.apsusc.2018.08.126>
5. Fang J, Fan H, Tian H, Dong G (2015) Morphology control of ZnO nanostructures for highly efficient dye-sensitized solar cells. *Mater Charact* 108:51–57. <https://doi.org/10.1016/j.matchar.2015.08.01>
 6. Gangadhar G, Maheshwari U, Gupta S (2012) Application of nanomaterials for the removal of pollutants from effluent water streams. *JNN* 2:140–150. <https://doi.org/10.2174/2210681211202020140>
 7. Nekouei F, Noorzadeh H, Nekouei S, Asif M, Tyagi I, Agarwal S, Gupta VK (2015) Removal of malachite green from aqueous solutions by cuprous iodide-cupric oxide nano-composite loaded on activated carbon as a new sorbent for solid phase extraction: isotherm, kinetics and thermodynamic studies. *J Mol Liq*. <https://doi.org/10.1016/j.molliq.2015.07.058>
 8. Mahdavi S, Jalai M, Afkhami A (2012) Heavy metals removal from aqueous solutions using TiO₂, MgO and Al₂O₃ nanoparticles. *Chem Eng Commun* 200(3):448–470. <https://doi.org/10.1080/00986445.2012.686939>
 9. Gautam RK, Sharma SK, Chattopadhyaya MC (2015) Functionalized magnetic nanoparticles for heavy metals removal from aqueous solutions. Royal Society of Chemistry, London, p 57
 10. Sharma YC, Srivastava V, Singh VK, Kaul SN, Weng CH (2009) Nano-adsorbents for the removal of metallic pollutants from water and wastewater. *Environ Technol* 30(6):583–609. <https://doi.org/10.1080/09593330902838080>
 11. Kamberg ML (2010) The Transition elements: the 38 transition metals. The Rosen Publishing Group, New York
 12. Zahar MS, Kusin FM, Muhammad SN (2015) Adsorption of manganese in aqueous solution by steel slag. *Procedia Environ Sci* 30:145–150. <https://doi.org/10.1016/j.proenv.2015.10.026>
 13. Al-Rashdi B, Somerfield C, Hilal N (2011) Heavy metals removal using adsorption and nanofiltration techniques. *Sep Purif Rev* 40:209–259. <https://doi.org/10.1080/15422119.2011.558165>
 14. Barakat MA, Kumar R (2015) Modified and new adsorbents for removal of heavy metals from wastewater. *R S Chem*. <https://doi.org/10.1039/9781782620174-00193>
 15. Jiang Y, Shuyan G, Zhengdao L, Xiaoxia J, Chen Y (2011) Cauliflower-like CuI nanostructures: green synthesis and applications as catalyst and adsorbent. *Mater Sci Eng B* 176:1021–1027. <https://doi.org/10.1016/j.mseb.2011.05.023>
 16. Ghanbari M, Bazarganipour M, Salavati-Niasari M (2017) Photodegradation and removal of organic dyes using CuI nanostructures, green synthesis and characterization. *Sep Purif Technol* 173:27–36. <https://doi.org/10.1016/j.seppur.2016.09.003>
 17. Hua-Jian X, Yu-Feng L, Zhen-Ya C, Hong-Xia Q, Chun-Yan Y, Yi-Si F (2011) CuI-nanoparticles-catalyzed selective synthesis of phenols, anilines, and thiophenols from aryl halides in aqueous solution. *J Org Chem* 76:2296–2300. <https://doi.org/10.1021/jo102506x>
 18. Gaveshana A, Steffen M, Alexander P, Andrew D, Fuzhi H, Udo B et al (2015) Copper(I) iodide as hole-conductor in planar perovskite solar cells: probing the origin of J–V hysteresis. *Adv Funct Mater* 25:5650–5661. <https://doi.org/10.1002/adfm.201502541>
 19. Indubala E, Dhanasekar M, Sudha V, Revathy R, Venkataprasad Bhat S, Harinipriya S et al (2018) L-Alanine capping of ZnO nanorods: increased carrier concentration in ZnO/CuI heterojunction diode. *RSC Adv* 8:5350–5361. <https://doi.org/10.1039/C7RA12385J>
 20. Camila S, Anthony Mennito S, Bethany Wolf J, David Pashley H, Walter Renné G (2015) Incorporation of bactericidal poly-acrylic acid modified copper iodide particles into adhesive resins. *J Dent* 43:546–555. <https://doi.org/10.1016/j.jdent.2015.02.012>
 21. Sekkal W, Zaoui A (2002) Monte Carlo study of transport properties in copper halides. *Physica B* 315:201–209. [https://doi.org/10.1016/S0921-4526\(01\)01043-2](https://doi.org/10.1016/S0921-4526(01)01043-2)
 22. Feraoun H, Aourag H, Certier M (2003) Theoretical studies of substoichiometric CuI. *Mater Chem Phys* 82:597–601. [https://doi.org/10.1016/S0254-0584\(03\)00318-3](https://doi.org/10.1016/S0254-0584(03)00318-3)
 23. Ferhat M, Zaoui A, Certier M, Dufour JP, Kgelifa B (1996) Electronic structure of the copper halides CuCl, CuBr and CuI. *Mater Sci Eng B* 39:95–100. [https://doi.org/10.1016/0921-5107\(95\)01518-3](https://doi.org/10.1016/0921-5107(95)01518-3)
 24. Chen D, Wang Y, Lin Z, Huang J, Chen X, Pan D (2010) Growth strategy and physical properties of the high mobility P-type CuI crystal. *Cryst Growth Des* 10:2057–2060. <https://doi.org/10.1021/cg100270d>
 25. Dhere SL, Latthe SS, Kappenstein C, Mukherjee SK, Rao AV (2010) Comparative studies on p-type CuI grown on glass and copper substrate by SILAR method. *Appl Surf Sci* 256:3967–3971. <https://doi.org/10.1016/j.apsusc.2010.01.058>
 26. Meng LR, Mo R, Zhou H, Wang G, Chen W, Wang D (2010) Synthesis of luminescent cubic phase one-dimensional CuI nanostructures in solution. *Cryst Growth Des* 10:3387–3390. <https://doi.org/10.1021/cg9015417>
 27. Tanji A, Akai I, Kojima K, Karasawa T, Komatsu T (2000) Exciton transitions in the hexagonal CuI microcrystallites grown on polymers. *J Lumin* 87:516–518. [https://doi.org/10.1016/S0022-2313\(99\)00274-4](https://doi.org/10.1016/S0022-2313(99)00274-4)
 28. Tennakone K, Kumara GRRA, Kottegoda IRM, Perera VPS, Aponso GMLP, Wijayantha KGU (1998) Deposition of thin conducting films of CuI on glass. *Sol Energy Mater Sol Cells* 55:283–289. [https://doi.org/10.1016/S0927-0248\(98\)00117-2](https://doi.org/10.1016/S0927-0248(98)00117-2)
 29. Liu Y, Zhan J, Zeng J, Qian Y, Tang K, Yu W (2001) Ethanolthermal synthesis to γ -CuI nanocrystals at low temperature. *J Mater Sci Lett* 20:1865–1867. <https://doi.org/10.1023/A:1012849522970>
 30. Ishak Afşin K (2016) CuI film produced by chemical extraction method in different media. *Mater Res* 19(5):991–998. <https://doi.org/10.1590/1980-5373-MR-2016-0067>
 31. Grajeda-Iglesias C, Figueroa-Espinoza M, Barouh N, Baréa B, Fernandes A, de Freitas V (2016) Isolation and characterization of anthocyanins from *Hibiscus sabdariffa* flowers. *J Nat Prod* 79:1709–1718. <https://doi.org/10.1021/acs.jnatprod.5b00958>
 32. Tavakoli F, Salavati-Niasari M, Mohandes F (2013) Green synthesis of flower-like CuI microstructures composed of trigonal nanostructures using pomegranate juice. *Mater Lett* 100:133–136. <https://doi.org/10.1016/j.matlet.2013.02.114>
 33. Prakash T (2011) Influence of temperature on physical properties of copper (I) iodide. *Adv Mater Lett* 2(2):131–135. <https://doi.org/10.5185/amlett.2011.1208>
 34. Pishchev A, Zh Karazhanov S (2017) Structure-property relationships in cubic cuprous iodide: a novel view on stability, chemical bonding, and electronic properties. *J Chem Phys* 146:064706(1)–064706(12). <https://doi.org/10.1063/1.4975176>
 35. Gao P, Gu M, Liu XL, Liu B, Huang SM (2009) X-ray excited luminescence of cuprous iodide single crystals: on the nature of red luminescence. *Appl Phys Lett* 95:221904(1)–221904(3). <https://doi.org/10.1063/1.3271174>
 36. Gruzintsev AN, Zagorodnev WN (2012) Effect of annealing on the luminescence of p-CuI crystals. *Semiconductors* 46:149–154.
 37. Foo KY, Hamed BH (2010) Insights into the modelling of adsorption isotherm system. *Chem Eng J* 156:2–10. <https://doi.org/10.1016/j.cej.2009.09.013>
 38. Bishnoi NR, Bajaj M, Sharma N, Gupta A (2004) Adsorption of Cr(VI) on activated rice husk carbon and activated alumina. *Bioresour Technol* 91:305–307. [https://doi.org/10.1016/S0960-8524\(03\)00204-9](https://doi.org/10.1016/S0960-8524(03)00204-9)

39. Jing H, Guohua C, Irene Lo MC, Asce M (2006) Selective removal of heavy metals from industrial wastewater using maghemite nanoparticle: performance and mechanisms. *J Environ Eng* 132:709–715. [https://doi.org/10.1061/\(ASCE\)0733-9372\(2006\)132:7\(709\)](https://doi.org/10.1061/(ASCE)0733-9372(2006)132:7(709))
40. Sharma YC, Srivastava V, Mukherjee AK (2010) Synthesis and application of nano- Al_2O_3 powder for the reclamation of Hexavalent chromium from aqueous solutions. *J Chem Eng Data* 55:2390–2398. <https://doi.org/10.1021/jc900822j>
41. Ahmad BA, Chirangano M, Ala'a H, Gavin MW, Stephen JA, Mohammad NM (2012) Kinetic and thermodynamics of chromium ions adsorption onto low-cost dolomite adsorbent. *Chem Eng J* 179:193–202. <https://doi.org/10.1016/j.cej.2011.10.080>
42. Jing H, Irene Lo MC, Chen G (2005) Fast removal and recovery of Cr(VI) using surface-modified jacobsite (MnFe_2O_4) nanoparticles. *Langmuir* 21:11173–11179. <https://doi.org/10.1021/la051076h>
43. Runhu Z, Wang B, Hongzhu M (2010) Studies on chromium (VI) adsorption on sulfonated lignite. *Desalination* 255:61–66. <https://doi.org/10.1016/j.desal.2010.01.016>
44. Parlayici S, Eskizeybek V, Ahmet A, Pehlivan Erol (2015) Removal of chromium (VI) using activated carbon-supported functionalized carbon nanotubes. *J Nanostruct Chem* 5:255–263. <https://doi.org/10.1007/s40097-015-0156-z>
45. Ucer A, Uyanik A, Aygun ŞF (2006) Adsorption of Cu (II), Cd (II), Zn (II), Mn(II) and Fe(III) ions by tannic acid immobilised activated carbon. *Sep Purif Technol* 47:113–118. <https://doi.org/10.1016/j.seppur.2005.06.012>
46. Rajic N, Stojakovic D, Jevtic S, Zabukovec Logar N, Kovacc J, Kaucic V (2009) Removal of aqueous manganese using the natural zeolitic tuff from the Vranjska Banja deposit in Serbia. *J Hazard Mater* 172:1450–1457. <https://doi.org/10.1016/j.jhazmat.2009.08.011>
47. Yan H, Li H, Tao X, Li K, Yang H, Li A (2014) Rapid removal and separation of iron (II) and manganese (II) from micro polluted water using magnetic graphene oxide. *Appl Mater Interfaces* 6(12):9871–9880. <https://doi.org/10.1021/am502377n>
48. Zhenze L, Shigeyoshi I, Takeshi K, Toru I, Xiaowu T, Qiang T (2010) Manganese removal from aqueous solution using a thermally decomposed leaf. *J Hazard Mater* 177:501–507. <https://doi.org/10.1016/j.jhazmat.2009.12.061>
49. Emmanuela KA, Veerabhadra Rao A (2008) Adsorption of Mn (II) from aqueous solutions using Pithacelobium Dulce carbon. *Rasayan J Chem* 1:840–852
50. Vijayaraghavan K, Heng Yun Ni W, Balasubramanian R (2011) Biosorption characteristics of crab shell particles for the removal of manganese (II) and zinc (II) from aqueous solutions. *Desalination* 266:195–200. <https://doi.org/10.1016/j.desal.2010.08.026>
51. Vaghetti JCP, Lima EC, Royer B, da Cunha BM, Cardoso NF, Brasil JL (2009) Pecan nutshell as biosorbent to remove Cu (II), Mn(II) and Pb(II) from aqueous solutions. *J Hazard Mater* 162:270–280. <https://doi.org/10.1016/j.jhazmat.2008.05.039>

Publisher's Note Springer Nature remains neutral with regard to jurisdictional claims in published maps and institutional affiliations.